Extracting 3D Structures from Biomedical Data

Xianghua Xie
College of Science
Swansea University
Talbot Building, Singleton Park, Swansea SA2 8PP,
United Kingdom.
Email: x.xie@swansea.ac.uk

Si Yong Yeo, Igor Sazonov, and Perumal Nithiarasu
College of Engineering
Swansea University
Talbot Building, Singleton Park, Swansea SA2 8PP,
United Kingdom.
Email: {465186, i.sazonov, p.nithiarasu}@swansea.ac.uk

Abstract—We present a 3D deformable model that is based on a geometrically induced external force field which can be conveniently generalized to arbitrary dimensions. This external force field is based on hypothesized interactions between the relative geometries of the deformable model and the object boundary characterized by image gradient. The evolution of the deformable model is solved using the level set method so as to facilitate topological changes. The proposed external force field can attract the deformable model to object boundaries with arbitrary initialization, and allows the deformable model to reach highly concave regions which are generally difficult for other methods. We provide a comparative study on the segmentation of various geometries in real 3D images, and show that the proposed method achieves significant improvements against existing image gradient techniques.

Index Terms—Deformable model, 3D image segmentation, biomedical image processing, level set, energy minimization.

I. INTRODUCTION

Segmenting volumetric biomedic data is an intricate process, due to the complexity and variability of image data and shapes. There have been applications of simple techniques such as thresholding and region growing in the extraction of 3D objects from volumetric images. However, these techniques are very sensitive to noise and intensity inhomogeneities which exist in real images, and often produce leakages and regions which are not contiguous. Atlas based approaches perform segmentation based on image registration techniques, whereby an image can be segmented by finding a transformation that maps a template image to the target image. It is however generally difficult to accurately extract complex geometries due to the variability of anatomical structures. Statistical approaches [1] are also used to identify different tissue structures from medical images. It usually involves manual interaction to segment images in order to obtain a sufficiently large set of training samples. Such strategies are often restricted to problems where there is sufficient prior knowledge about the shape or appearance variations of the relevant structures.

Deformable models can be an effective alternative approach. They are usually based on a variational framework to minimize an energy functional defined on a continuous contour or surface. They have the ability to adapt to complex shape variations and to incorporate priors to regularize segmentation. Curves or surfaces evolve under the influence of both internal and external forces to extract the image object boundaries. The design of deformable models often varies in the representation of the object boundary and external force field used. These usually take the form of image gradient based approaches e.g. [2]–[5], region based approaches e.g. [6], [7] and hybrid approaches e.g. [8]. Image gradient based techniques have been found useful when there is limited prior knowledge and image gradients are reasonable indications of object boundaries. However, the extension from 2D to 3D is not trivial. Conventional image gradient based approaches, such as [2], require careful initialization even in 2D. This is especially true when segmenting objects with complex geometries and shapes in 3D, where delicate manual initialization is even more difficult than in 2D.

Region based methods [6], [7], [9], [10] have also been widely applied to image segmentation. The Chan-Vese model [6] which is based on the Mumford-Shah functional [11] is considered as one of the most popular region based techniques. In this approach, the image is assumed to be composed of regions of approximately piecewise-constant intensities. The Chan-Vese model then extracts the image object based on the average intensities inside and outside the contour. Although the Chan-Vese model can be used to extract objects with smoothly varying boundaries, it has difficulties dealing with image regions with intensity inhomogeneity. Other region based models such as [10] also assume that image objects consist of distinct regional features, which is often not true for real image dataset due to intensity inhomogeneity and multi-modal nature.

II. PROPOSED METHOD

Our approach is to define a novel external force field that is based on hypothesized geometrically induced interactions between the relative geometries of the deformable model and the object boundaries (characterized by image gradients). In other words, the magnitude and direction of the interaction forces are based on the relative position and orientation between the geometries of the deformable model and image object boundaries, and hence, it is called the *geometric potential force (GPF)* field. The bidirectionality of the new external force field can facilitate arbitrary cross-boundary initialization, which is a very useful feature to have, especially in the segmentation of complex geometries in 3D. It also improves the performance of the deformable model in handling weak edges. In addition, the
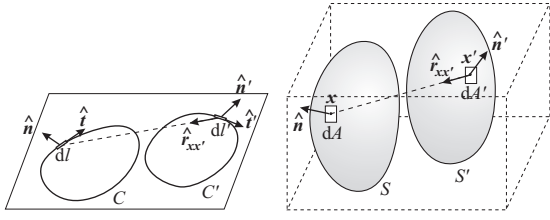
Fig. 1. Relative position and orientation between geometries in 2D and 3D.

proposed external force field is dynamic in nature as it changes according to the relative position and orientation between the evolving deformable model and object boundary.

In order to first deduce the geometric interaction force in 2D, consider a deformable contour C and an ideal object boundary C' in the image plane (see Fig. 1). Let $\mathrm{d}l$ and $\mathrm{d}l'$ denote the infinitesimal elements of contour C and object boundary C', respectively. In the existing force field based models such as [12], [13], the interaction between $\mathrm{d}l$ and $\mathrm{d}l'$ is inversely proportional to the distance separating these two elements and the derived force lies in a straight line between them. They do not take into account the local geometry of the deformable contour C or object boundary C'. We propose to incorporate the mutual location and orientation of these elements.

Let $\boldsymbol{x}$ and $\boldsymbol{x}'$ denote the positions of elements $\mathrm{d}l$ and $\mathrm{d}l'$, respectively. Thus, $\boldsymbol{r}_{\boldsymbol{x}\boldsymbol{x}'} = \boldsymbol{x} - \boldsymbol{x}'$ is their mutual location of those two elements, $r_{\boldsymbol{x}\boldsymbol{x}'} = |\boldsymbol{x} - \boldsymbol{x}'|$ is the distance between them, and $\hat{\boldsymbol{r}}_{\boldsymbol{x}\boldsymbol{x}'} = (\boldsymbol{x} - \boldsymbol{x}')/r_{\boldsymbol{x}\boldsymbol{x}'}$ is the unit vector pointing $\mathrm{d}l$ from $\mathrm{d}l'$. The directions of these elements can be represented by their unit tangent vectors $\hat{\boldsymbol{t}}$ and $\hat{\boldsymbol{t}}'$. However, a unique tangent vector is no longer available for infinitesimal surface elements in 3D. Thus, we use unit outward normal vectors $\hat{\boldsymbol{n}}$ and $\hat{\boldsymbol{n}}'$ to characterize the orientations of these elements instead (see Fig. 1). In 2D, they are simply 90° rotated tangent vectors.

We are now ready to introduce the hypothesized interaction force $\mathrm{d}\mathbf{F}\,\mathrm{d}l$ which acts on element $\mathrm{d}l$ by virtue of the hypothesized force field induced by element $\mathrm{d}l'$. It is desirable to combine the element orientation vectors and distance vector in deriving the force. We propose a simple but effective combination of these three vectors as $\hat{\boldsymbol{n}}\,(\hat{\boldsymbol{r}}_{\boldsymbol{x}\boldsymbol{x}'} \cdot \hat{\boldsymbol{n}}')$. The multiplication of contour normal $\hat{\boldsymbol{n}}$ ensures that the force is always imposed in the normal direction so that the deformable model does not suffer from convergence issues (i.e. stationary points, saddle points and extreme boundary concavities), which are often associated with other vector force field based methods such as GGVF [3]. The dot product of the object boundary element normal with the distance vector allows the force on the contour in the normal direction to diminish as the contour reaches the object boundary. Similar to other physics-inspired force field, it is also desirable to decay the force interaction with the increase of distance between the elements, i.e. the force is designed proportional to $\hat{\boldsymbol{n}}\,(\hat{\boldsymbol{r}}_{\boldsymbol{x}\boldsymbol{x}'} \cdot \hat{\boldsymbol{n}}')/r^{\lambda}_{\boldsymbol{x}\boldsymbol{x}'}$ where $\lambda > 0$. Thus, the contribution of element $\mathrm{d}l'$ of object boundary C' to the total force acting on $\mathrm{d}l$ in accordance with their distance

and mutual orientation can be formulated as

$$\mathrm{d}\mathbf{F}\,\mathrm{d}l = \hat{\boldsymbol{n}}\,\mathrm{d}G\,\mathrm{d}l, \qquad \mathrm{d}G = \left(\frac{\hat{\boldsymbol{r}}_{\boldsymbol{x}\boldsymbol{x}'}}{r^{\lambda}_{\boldsymbol{x}\boldsymbol{x}'}} \cdot \hat{\boldsymbol{n}}'\right)\mathrm{d}l' \qquad (1)$$

where $\mathbf{F}$ is defined as force per unit length, $\mathrm{d}G$ is the contribution of element $\mathrm{d}l'$ of object boundary C' into the scalar field $G(\boldsymbol{x})$, which can be considered as an intermediate potential field, and λ is a positive constant that affects the magnitude of the interaction force based on the distance between the elements. In our study we obtained the best results when λ coincides with the dimension of the image data, i.e. $\lambda = 2$ in the 2D case. Furthermore, we show later that when λ coincides with data dimension in 2D, the proposed force interaction has an explicit link to the magnetostatics theory and thus the spatial decay of the magnitude of the interaction force is analogous to that of the magnetic field.

In real images, ∇I is a smooth function reaching maximum of its magnitude in vicinity of the object boundary. The geometric potential field in a continuous form can then be formulated as

$$G(\boldsymbol{x}) = P.V. \iiint\limits_{\Omega} \left(\frac{\hat{\boldsymbol{r}}_{\boldsymbol{x}\boldsymbol{x}'}}{r^{\lambda}_{\boldsymbol{x}\boldsymbol{x}'}} \cdot \nabla I(\boldsymbol{x}')\right)\mathrm{d}V'. \qquad (2)$$

Note, due to the substitution of $\mathcal{W}(\boldsymbol{x}')\,\hat{\boldsymbol{n}}'(\boldsymbol{x}')\,\delta(\boldsymbol{x}'' - \boldsymbol{x}')$ by $\nabla I(\boldsymbol{x}'')$, the $\boldsymbol{x}'$ defined on the ideal surface S' is no longer needed. Hence, the notation is simplified by replacing the integral variable $\boldsymbol{x}''$ with $\boldsymbol{x}'$. Finally, its discrete form can be written as

$$G(\boldsymbol{x}) = \sum_{\boldsymbol{x}' \in \Omega, \boldsymbol{x}' \neq \boldsymbol{x}} \left(\frac{\hat{\boldsymbol{r}}_{\boldsymbol{x}\boldsymbol{x}'}}{r^{\lambda}_{\boldsymbol{x}\boldsymbol{x}'}} \cdot \nabla I(\boldsymbol{x}')\right). \qquad (3)$$

This can be considered as a convolution of the image gradient with the vector kernel $\mathbf{K}_{\lambda}(\boldsymbol{x})$

$$\begin{cases} \mathbf{K}_{\lambda}(\boldsymbol{x}) = P.V. \dfrac{\hat{\boldsymbol{x}}}{|\boldsymbol{x}|^{\lambda}} = P.V. \dfrac{\boldsymbol{x}}{|\boldsymbol{x}|^{\lambda+1}} \\[2mm] G = \mathbf{K}_{\lambda} * \nabla I = \iiint\limits_{\Omega} \left(\mathbf{K}_{\lambda}(\boldsymbol{x} - \boldsymbol{x}') \cdot \nabla I(\boldsymbol{x}')\right) dV' \end{cases} \qquad (4)$$

which can be carried out efficiently using the fast Fourier transform (FFT). Note that the potential field G is computed as a convolution of two vector functions.

The total force acting on the unit area element of the deformable surface S is thus given as $\mathbf{F} = \hat{\boldsymbol{n}}\,G(\boldsymbol{x})$. where $\hat{\boldsymbol{n}}$ is the outward unit normal of level set surface. Note, an inward normal can also be used, i.e. $\mathbf{F} = -\hat{\boldsymbol{n}}\,G(\boldsymbol{x})$, which will result in opposite deformable model propagation since the force field is exactly in the opposite direction. Hence, the force can be re-written in a generalized form:

$$\mathbf{F} = \mathcal{J}\hat{\boldsymbol{n}}\,G(\boldsymbol{x}). \qquad (5)$$

where $\mathcal{J}$ is a constant taking values of ± 1.

Once the force field $\mathbf{F}(\boldsymbol{x})$ is derived from the hypothesized interactions based on the relative geometries of the deformable model and object boundary is determined, the evolution of the

deformable model $S(\boldsymbol{x}, t)$ under this GPF field can be given as

$$\frac{\mathrm{d}S}{\mathrm{d}t} = (\mathbf{F} \cdot \hat{\boldsymbol{n}})\hat{\boldsymbol{n}}. \tag{6}$$

Since surface smoothing is usually desirable, the mean curvature flow can be incorporated and the complete GPF deformable model evolution can be formulated as

$$\frac{\mathrm{d}S}{\mathrm{d}t} = \alpha \, g \, \kappa \, \hat{\boldsymbol{n}} + (1 - \alpha)(\mathbf{F} \cdot \hat{\boldsymbol{n}})\hat{\boldsymbol{n}} \tag{7}$$

where $g(\boldsymbol{x}) = 1/(1 + |\nabla I|)$ is the edge stopping function. Note that in our case, the flow of $\mathbf{F}$ is directed by definition normal to surface S, therefore $(\mathbf{F} \cdot \hat{\boldsymbol{n}})\hat{\boldsymbol{n}} = \mathbf{F}$. Notation $(\mathbf{F} \cdot \hat{\boldsymbol{n}})\hat{\boldsymbol{n}}$ is inherited from the traditional methods. The level set representation of the proposed deformable model based on GPF can then be written as

$$\frac{\partial \Phi}{\partial t} = \alpha \, g \, \kappa \, |\nabla \Phi| - (1 - \alpha)(\mathbf{F} \cdot \nabla \Phi) \tag{8}$$

where $\Phi(t, \boldsymbol{x})$ is the level set function, such that the deformable surface S is defined as $\Phi(t, \boldsymbol{x}) = 0$. Note, the GPF force field is defined on the deformable surface, which is implicitly embedded in the level set function, i.e. the force field computed at the propagating front needs to be extended across the computational domain so that the full level set function can be continuously evolved.

Although the GPF deformable model can reduce its noise sensitivity to a certain extent by modeling gradient vector interactions across the image domain, deformable models based on image gradients are in general susceptible to heavy noise interference. Note, the GPF force $\mathbf{F}$ is determined by its potential G, see (5), and G can be pre-computed before evolving the deformable model. Thus, we can improve its performance towards image noise by refining the potential G. Here, we enhance it using non-local methods [14], [15], so as to increase its robustness even in the presence of a large amount of image noise.

Given the noisy image $I(\boldsymbol{x})$ and its corresponding geometric potential field $G(\boldsymbol{x})$, this non-local smoothing of the geometric potential field is carried out by computing a weighted average at each voxel position $\boldsymbol{x}$ according to:

$$G'(\boldsymbol{x}) = \sum_{\boldsymbol{x}' \in \Omega_{\boldsymbol{x}}, \boldsymbol{x}' \neq \boldsymbol{x}} w(\boldsymbol{x}, \boldsymbol{x}') \, G(\boldsymbol{x}) \tag{9}$$

where $\Omega_{\boldsymbol{x}}$ is a search window centered around $\boldsymbol{x}$. Following the approach in Buades *et al.* [14], we measure the similarity between two square (2D) or cube (3D) regions centered at location $\boldsymbol{x}$ and $\boldsymbol{x}'$, and determine the similarity weight from the image $I(\boldsymbol{x})$ as:

$$w(\boldsymbol{x}, \boldsymbol{x}') = \frac{1}{Z(\boldsymbol{x})} e^{-\frac{1}{h^2}\left(\sum_{\delta \in \boldsymbol{N}} G_\sigma(\delta)(I(\boldsymbol{x}+\delta) - I(\boldsymbol{x}'+\delta))^2\right)^2} \tag{10}$$

where $G_\sigma(.)$ is a Gaussian kernel with standard deviation σ, $\boldsymbol{N}$ denotes the region containing the pixels/voxels location δ, h is the parameter that controls the amount of filtering, and $Z(\boldsymbol{x})$ is a normalization constant given by $Z(\boldsymbol{x}) = \sum_{\boldsymbol{x}' \in \Omega_{\boldsymbol{x}}} w(\boldsymbol{x}, \boldsymbol{x}')$.
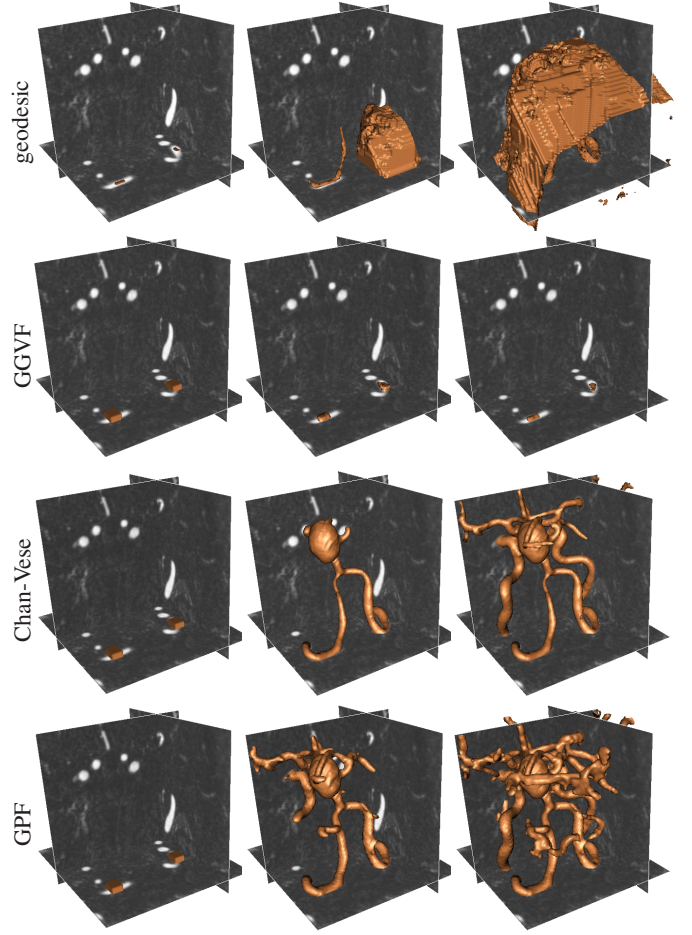

Fig. 2. Segmentation of cerebral arterial structure from MR image dataset using different deformable models - first row: geodesic; second row: GGVF; third row: Chan-Vese; fourth row: proposed GPF.

The force acting due to the enhanced geometrical potential field on the deformable surface S described in (5) can then be given as:

$$\begin{aligned} \mathrm{d}\mathbf{F}(\boldsymbol{x}) &= \mathcal{J} \, \mathrm{d}A_1 \, \hat{\boldsymbol{n}}(\boldsymbol{x}) \, G'(\boldsymbol{x}) \\ &= \mathcal{J} \, \mathrm{d}A_1 \, \hat{\boldsymbol{n}}(\boldsymbol{x}) \sum_{\boldsymbol{x}' \in \Omega_{\boldsymbol{x}}, \boldsymbol{x}' \neq \boldsymbol{x}} w(\boldsymbol{x}, \boldsymbol{x}') \, G(\boldsymbol{x}) \end{aligned} \tag{11}$$

By comparing regional similarity instead of single pixel/voxel similarity from the noisy image, a more reliable geometric potential field is achieved. Moreover, oscillations at flat or homogeneous regions are readily smoothed and edge information at object boundaries are enhanced in the denoised geometric potential field.

III. RESULTS

In this section, we present experimental results on real 3D image data. The comparative analysis is performed using several classical and state-of-the-art methods which consists of image gradient based and region based methods.

Real images often contain complex geometries and topologies, image noise and weak edges. Here, we show some

comparative results on the segmentation of 3D medical data. Fig. 2 shows comparative results on the segmentation of cerebral arterial structure from magnetic resonance (MR) imaging. Two initial surfaces are placed inside the object of interest for the geodesic model, and across the object boundaries for GGVF [3] (generalized and improved GVF), Chan-Vese [6] and GPF. The geodesic model cannot propagate through the narrow tubular structures, and leaks out at weak object boundaries during the evolution. The GGVF model collapsed to the nearby object edges due to the saddle or stationary points inside the narrow image structures. In contrast, the Chan-Vese and GPF models are able to propagate through the long tubular structures to extract the cerebral arterial geometry. Fig. 3 presents another example whereby a femur is segmented from CT images using the different methods. In this example, the geodesic model and the Chan-Vese model leaked due to the weak image edges and varying intensities respectively, while the GGVF and EI [16] models had difficulties in propagating across the image object. The GPF model, however, can effectively extract the image object despite the image noise, weak edges and inhomogeneous intensities. The improvements achieved by the proposed method, as demonstrated extensively in various examples, are significant and consistent.

IV. CONCLUSION

We have presented a 3D deformable model that uses an external force field known as the geometric potential force (GPF), which is computed based on the relative geometrical configurations between the deformable model and image object. The method utilizes voxel interactions across the whole image, which effectively provides a global representation of the image object. The derived geometric potential field is thus more informative and exhibits spatial and structural characteristics of image objects which are more coherent than image cues that are based solely on local edge or regional information. This makes the model more robust towards image noise and weak object edges.
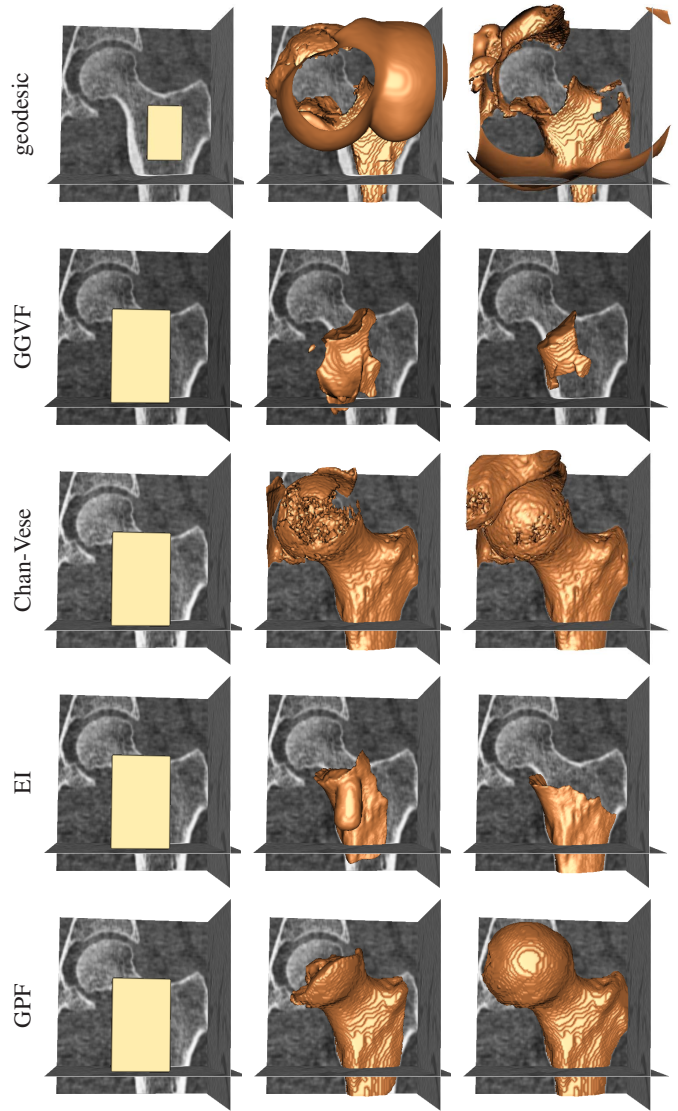

Fig. 3. Segmentation of femur from CT image dataset using different deformable models - first row: geodesic; second row: GGVF; third row: Chan-Vese; fourth row: EI; fifth row: proposed GPF.

REFERENCES

[1] J. Hao and M. Li, "A supervised bayesian method for cerebrovascular segmentation," *WSEAS Trans. Signal Processing*, vol. 3, no. 12, pp. 487–495, 2007.

[2] R. Malladi, J. A. Sethian, and B. C. Vemuri, "Shape modelling with front propagation: A level set approach," *IEEE T-PAMI*, vol. 17, no. 2, pp. 158–175, 1995.

[3] C. Xu and J. L. Prince, "Generalized gradient vector flow external forces for active contours," *Signal Processing*, vol. 71, no. 2, pp. 131–139, 1998.

[4] X. Xie and M. Mirmehdi, "MAC: Magnetostatic active contour model," *IEEE T-PAMI*, vol. 30, no. 4, pp. 632–647, 2008.

[5] X. Xie, "Active contouring based on gradient vector interaction and constrained level set diffusion," *IEEE T-IP*, vol. 19, no. 1, pp. 154–164, 2010.

[6] T. Chan and L. Vese, "Active contours without edges," *IEEE T-IP*, vol. 10, no. 2, pp. 266–277, 2001.

[7] D. Cremers, M. Rousson, and R. Deriche, "A review of statistical approaches to level set segmentation: Integrating color, texture, motion and shape," *IJCV*, vol. 72, no. 2, pp. 195–215, 2007.

[8] X. Xie and M. Mirmehdi, "RAGS: Region-aided geometric snake," *IEEE T-IP*, vol. 13, no. 5, pp. 640–652, 2004.

[9] L. Vese and T. Chan, "A multiphase level set framework for image segmentation using the mumford and shah model," *IJCV*, vol. 50, no. 3, pp. 271–293, 2002.

[10] J. Kim, J. W. Fisher, A. Yezzi, M. Cetin, and W. A. S., "A nonparametric statistical method for image segmentation using information theory and curve evolution," *IEEE T-MI*, vol. 14, no. 10, pp. 1486–1502, 2005.

[11] D. Mumford and J. Shah, "Optimal approximations by piecewise smooth functions and associated variational problems," *Communications on Pure and Applied Mathematics*, vol. 42, no. 5, pp. 577–685, 1989.

[12] R. Yang, M. Mirmehdi, and X. Xie, "A charged active contour based on electrostatics," in *ACIVS*, 2006, pp. 173–184.

[13] B. Li and S. Acton, "Active contour external force using vector field convolution for image segmentation," *IEEE T-IP*, vol. 16, no. 8, pp. 2096–2106, 2007.

[14] A. Buades, B. Coll, and J. Morel, "A non-local algorithm for image denoising," in *CVPR*, 2005, pp. 60–65.

[15] J. Darbon, A. Cunha, T. Chan, S. Osher, and G. Jensen, "Fast nonlocal filtering applied to electron cryomicroscopy," in *IEEE Int. Symposium on Biomed. Imag.: From Nano to Macro*, 2008, pp. 1331–1334.

[16] Y. Xiang, A. Chung, and J. Ye, "An active contour model for image segmentation based on elastic interaction," *J. Comp. Phy.*, vol. 219, no. 1, pp. 455–476, 2006.